Di-lepton production at STAR

Lijuan Ruan for the STAR Collaboration
Physics Department, Brookhaven National laboratory, Upton NY 11973

The recent results on di-electron production in $p+p$ and Au+Au collisions at $\sqrt{s_{NN}} = 200$ GeV are presented. The cocktail simulations of di-eletrons from light flavor meson decays and heavy flavor decays are reported and compared with data. The perspectives for di-lepton measurements in lower energy Au+Au collisions and with future detector upgrades are discussed.

1 Introduction

Ultra-relativistic heavy ion collisions provide a unique environment to study properties of strongly interacting matter at high temperature and high energy density [1]. One of the crucial probes of this strongly interacting matter are di-lepton measurements in the low and intermediate mass region. Di-leptons are not affected by the strong interaction once produced, therefore they can probe the whole evolution of the collision. The di-lepton spectra in the intermediate mass range ($1.1 < M_{ll} < 3.0$ GeV/c^2) are directly related to thermal radiation of the Quark-Gluon Plasma (QGP) [2,3]. In the low mass range ($M_{ll} < 1.1$ GeV/c^2), we can study vector meson in-medium properties through their di-lepton decays, where any modifications observed may relate to the possibility of chiral symmetry restoration.

Anisotropic flow, an anisotropy in the particle production relative to the reaction plane, leads to correlations among particles and have been studied by analysis of these correlations [4]. The elliptic flow v_2 is the second harmonic of the azimuthal distribution of particles with respect to the reaction plane. It is believed that di-lepton v_2 measurements will provide another independent way to study medium properties. Specifically, the v_2 as a function of transverse momentum (p_T) in different mass regions will enable us to probe the properties of medium from hadron-gas dominated to QGP dominated [5].

At STAR, the newly installed Time-of-Flight detector (TOF) offers high acceptance and efficiency [6]. The TOF, combined with measurements of ionization energy loss (dE/dx) from the Time Projection Chamber (TPC) [7,8,9], enables electron identification with high purity from low to intermediate p_T [10,11,12]. In this article we present the di-electron mass spectra in $p+p$ and Au+Au collisions at $\sqrt{s_{NN}} = 200$ GeV. The elliptic flow v_2 measurements are also reported in 200 GeV Au+Au collisions. Future capabilities for di-lepton measurements at STAR in lower energy Au+Au collisions and with detector upgrades are discussed.

2 Recent results on di-electron production

We utilize 107 million, 270 million and 150 million events for $p+p$, minimum-bias (0-80%) Au+Au, and central (0-10%) Au+Au di-electron analyses, respectively. The $p+p$ events were

taken in 2009 and 72% of the full TOF system was installed and operational while the Au+Au events were taken in 2010 with full TOF system coverage. By applying velocity and dE/dx cuts on tracks with $p_T > 0.2$ GeV/c, we can achieve the purity for the electron candidates at 99% in $p+p$ collisions and 97% in minimum-bias Au+Au collisions.

The di-electron signals may come from light flavor hadron decays and heavy flavor hadron decays, for example, π^0, η, and η' Dalitz decays: $\pi^0 \to \gamma e^+e^-$, $\eta \to \gamma e^+e^-$, and $\eta' \to \gamma e^+e^-$; vector meson decays: $\omega \to \pi^0 e^+e^-$, $\omega \to e^+e^-$, $\rho^0 \to e^+e^-$, $\phi \to \eta e^+e^-$, $\phi \to e^+e^-$, and $J/\psi \to e^+e^-$; heavy flavor decays: $c\bar{c} \to e^+e^-$ and $b\bar{b} \to e^+e^-$; and Drell-Yan contributions. In Au+Au collisions, we look for additional vector meson in-medium modifications in the low mass region and possible QGP thermal radiations in the intermediate mass range.

The e^+ and e^- pairs from the same events are combined to reconstruct the invariant mass distributions (M_{ee}) marked as unlike-sign distributions. The unlike-sign distributions contain both signal and background. The background contains the random combinatorial pairs and correlated pairs. The electron candidates are required to be in the range of $|\eta| < 1$ and $p_T > 0.2$ GeV/c while e^+e^- pairs are required to be in the rapidity range of $|y_{ee}| < 1$. Two methods are used for background estimation, based on same-event like-sign and mixed-event unlike-sign techniques. In the like-sign technique, electron pairs with the same charge sign are combined from the same events. In the mixed-event technique, unlike-sign pairs are formed from different events. In $p+p$ collisions, we subtract the like-sign background at $M_{ee} < 0.4$ GeV/c^2 and mixed-event background in the higher-mass region. In Au+Au collisions, we subtract the like-sign background at $M_{ee} < 0.7$ GeV/c^2 and mixed-event background in the higher-mass region. The detailed analysis procedures can be found in [13,14].

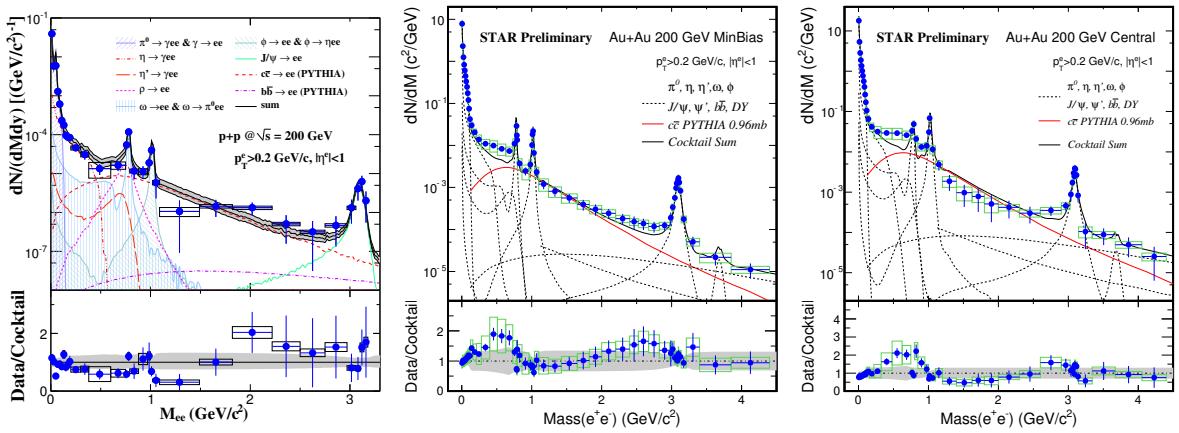

Figure 1: The comparison for di-electron continuum between data and simulation after efficiency correction within the STAR acceptance in $p+p$ (left panel), minimum-bias (middle panel) Au+Au and central (right panel) Au+Au collisions at $\sqrt{s_{NN}} = 200$ GeV. The di-electron continuum from simulations with different source contributions are also shown. The bars and boxes (bands) represent statistical and systematic uncertainties, respectively.

After the efficiency correction, the di-electron mass spectra within the STAR acceptance are shown in Fig. 1 for $p+p$, minimum-bias Au+Au and central Au+Au collisions at $\sqrt{s_{NN}} = 200$ GeV. The di-electron mass spectra are not corrected for momentum resolution and radiation energy loss effect. The ratios of data to cocktail simulations are shown in the lower panels. In $p+p$ collisions, the cocktail simulation, which includes the expected components from light flavor meson and heavy flavor meson decays, is consistent with the measured di-electron continuum within uncertainties. We also find that the $c\bar{c} \to e^+e^-$ contribution is dominant in the intermediate mass region. In Au+Au collisions, the ρ^0 contribution is not included and the $c\bar{c} \to e^+e^-$ contribution is from PYTHIA simulation, scaled by the number of underlying binary

nucleon-nucleon collisions. In the low mass region $0.15 < M_{ee} < 0.75$ GeV/c^2, the possible enhancement factors, the ratios of the data to the cocktail simulations, are $1.53 \pm 0.07 \pm 0.41$ and $1.72 \pm 0.10 \pm 0.50$ in minimum-bias and central collisions, respectively. This suggests for possible vector meson in-medium modification in this low mass region. Differential measurements as a function of p_T and centrality are on-going.

The di-lepton v_2 measurements provide another independent way to study the medium properties. We use event-plane method to obtain the di-electron v_2. The event-plane is reconstructed using the tracks from the TPC. The details of the method are in Refs. [4,15]. We report the v_2 of di-electron signals in Fig. 2 (left panel) as a function of M_{ee} in minimum-bias Au+Au collisions at $\sqrt{s_{NN}} = 200$ GeV. The differential v_2 of di-electron pairs in the mass regions of $M_{ee} < 0.14$ GeV/c^2 and $0.14 < M_{ee} < 0.30$ GeV/c^2 are shown in the middle and right panels of Fig. 2 as a function of p_T in minimum-bias Au+Au collisions at $\sqrt{s_{NN}} = 200$ GeV. Also shown are the charged [16] and neutral pion [17] v_2. The dominant contribution sources to di-electrons at $M_{ee} < 0.14$ GeV/c^2 and $0.14 < M_{ee} < 0.30$ GeV/c^2 are π^0 Dalitz decay and η Dalitz decay, respectively. We parameterize pion v_2 from low to high p_T, do the Dalitz decay simulation, and obtain the expected di-electron v_2 from π^0 Dalitz decay shown by the solid curve. The simulated v_2 is consistent with the measured di-electron v_2 at $M_{ee} < 0.14$ GeV/c^2. We repeat the same exercise in the η mass region. We assume that η has the same v_2 as K^0_S [15] since the mass of η is close to that of K^0_S. The simulated v_2 of di-electrons from η Dalitz decay, shown by the solid curve, is consistent with the measured di-electron v_2 at $0.14 < M_{ee} < 0.30$ GeV/c^2. The current precision of our v_2 data does not allow to further study a possible deviation from the solid curve due to the other contributions in this mass region. The consistency between the expectations and measurements demonstrates the credibility of our method to obtain the di-electron v_2.

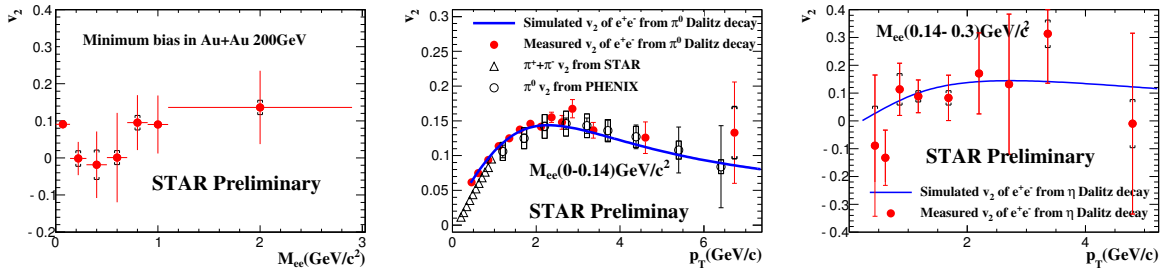

Figure 2: (left panel) The di-electron v_2 as a function of M_{ee} in minimum-bias Au+Au collisions at $\sqrt{s_{NN}} = 200$ GeV. (middle panel) The v_2 of di-electron at $M_{ee} < 0.14$ GeV/c^2 (solid symbol) as a function of p_T in minimum-bias Au+Au collisions at $\sqrt{s_{NN}} = 200$ GeV. Also shown are the charged and neutral pion v_2 and the expected v_2 (solid curve) of di-electrons from π^0 Dalitz decay. (right panel) The v_2 of di-electron at $0.14 < M_{ee} < 0.30$ GeV/c^2 as a function of p_T in minimum-bias Au+Au collisions at $\sqrt{s_{NN}} = 200$ GeV. Also shown is the expected v_2 (solid curve) of di-electrons from η Dalitz decay. The bars and boxes represent statistical and part of systematic uncertainties, respectively.

3 Future perspectives

A factor of two more data taken in 2011 will significantly improve the measurements of mass spectra and elliptic flow in Au+Au collisions at $\sqrt{s_{NN}} = 200$ GeV. In addition, in 2010 and 2011, STAR has taken a few hundred million minimum-bias events in Au+Au collisions at $\sqrt{s_{NN}} = 19.6, 27, 39, 62$ GeV with full TOF azimuthal coverage and low conversion material budget, which will enable us to systematically study the energy dependence of the following physics topics: 1) di-electron enhancement in the low mass region [18,19]; 2) in-medium modifications of vector meson decays; 3) virtual photons [20]; 4) $c\bar{c}$ medium modifications; and 5) possible QGP thermal radiation

in the intermediate mass region. With the current data sets, it will be difficult to measure 4) or 5) since they are coupled to each other and one is the other's background for the physics case. So far at RHIC, there is no clear answer about thermal radiation in the intermediate mass region. The future detector upgrade with the Heavy Flavor Tracker at STAR, to be completed in 2014, will provide precise charm cross section measurements [21], however the measurements of $c\bar{c}$ correlations will still be challenging if not impossible. An independent approach is proposed with the Muon Telescope Detector upgrade [22], $\mu - e$ correlations, to measure the contribution from heavy flavor correlations to the di-electron or di-muon continuum. This will make it possible to access the thermal radiation in the intermediate mass region.

4 Summary

In summary, the di-electron mass spectra are measured in 200 GeV $p+p$ and Au+Au collisions at STAR. The cocktail simulations are consistent with the data in 200 GeV $p+p$ collisions. In Au+Au collisions, we observe a possible enhancement by comparison between data and cocktail simulation in the low mass region $0.15 < M_{ee} < 0.75$ GeV/c^2. The first elliptic flow measurements of di-electrons are presented in 200 GeV minimum-bias Au+Au collisions. The v_2 of di-electrons at $M_{ee} < 0.14$ GeV/c^2 and $0.14 < M_{ee} < 0.30$ GeV/c^2 are in agreement with the expectations from previous measurements.

References

1. J. Adams *et al.*, Nucl. Phys. A **757**, 102 (2005).
2. R. Rapp and J. Wambach, Adv. Nucl. Phys. 25 (2000) 1.
3. G. David, R. Rapp and Z. Xu, Phys. Rept. **462**, 176 (2008).
4. A.M. Poskanzer and S.A. Voloshin, Phys. Rev. C **58**, 1671 (1998).
5. R. Chatterjee *et al.*, Phys. Rev. C **75**, 054909 (2007).
6. B. Bonner *et al.*, Nucl. Instr. Meth. A **508**, 181 (2003); M. Shao *et al.*, Nucl. Instr. Meth. A **492**, 344 (2002); J. Wu *et al.*, Nucl. Instr. Meth. A **538**, 243 (2005).
7. M. Anderson *et al.*, Nucl. Instr. Meth. A **499**, 659 (2003).
8. H. Bichsel, Nucl. Instr. Meth. A **562**, 154 (2006).
9. Y. Xu *et al.*, Nucl. Instr. Meth. A **614**, 28 (2010).
10. M. Shao *et al.*, Nucl. Instr. Meth. A **558**, 419 (2006).
11. J. Adams *et al.*, Phys. Lett. B **616**, 8 (2005).
12. J. Adams *et al.*, Phys. Rev. Lett. **94**, 062301 (2005).
13. L. Adamczyk *et al.*, arXiv:1204.1890; L. Ruan *et al.*, Nucl. Phys. A **855**, 269 (2011).
14. J. Zhao *et al.*, J. Phys. G **38**, 124134 (2011).
15. B.I. Abelev *et al.*, Phys. Rev. C **77**, 054901 (2008).
16. Y. Bai, Ph.D. Thesis, NIKHEF and Utrecht University, 2007, http://drupal.star.bnl.gov/STAR/files/Bai_Yuting.pdf .
17. S. Afanasiev *et al.*, Phys. Rev. C **80**, 054907 (2009).
18. A. Adare *et al.*, Phys. Rev. C **81**, 034911 (2010).
19. S. Afanasiev *et al.*, nucl-ex/0706.3034.
20. A. Adare *et al.*, Phys. Rev. Lett. **104**, 132301 (2010).
21. http://rnc.lbl.gov/hft/docs/hft_final_submission_version.pdf; S. Kleinfelder *et al.*, Nucl. Instr. Meth. A **565**, 132 (2006).
22. http://drupal.star.bnl.gov/STAR/system/files/MTD_proposal_v14.pdf; Z. Xu, BNL LDRD project 07-007; L. Ruan *et al.*, J. Phys. G **36**, 095001 (2009); Y. Sun et al., Nucl. Instr. Meth. A **593**, 307 (2008); Y. Wang et al., Nucl. Instr. Meth. A **640**, 85 (2011).